Adatom-mediated damage of two-dimensional materials under the electron beam in a transmission electron microscope

Mitisha Jain [1], Silvan Kretschmer [1], Jannik Meyer [2], and Arkady V. Krasheninnikov [1]
[1]*Institute of Ion Beam Physics and Materials Research, Helmholtz-Zentrum Dresden-Rossendorf, Bautzner Landstraße 400, 01328 Dresden, Germany*
[2]*Institute of Applied Physics, University of Tübingen, Auf der Morgenstelle 10, 72076 Tübingen, Germany*

(Received 29 January 2024; accepted 6 May 2024; published 24 May 2024)

The interaction of energetic electrons with the specimen during imaging in a transmission electron microscope (TEM) can give rise to the formation of defects or even complete destruction of the sample. This is particularly relevant to atomically thin two-dimensional (2D) materials. Depending on electron energy and material type, different mechanisms such as knock-on (ballistic) damage, inelastic interactions including ionization and excitations, as well as beam-mediated chemical etching can govern defect production. Using first-principles calculations combined with the McKinley-Feshbach formalism, we investigate damage creation in two representative 2D materials, MoS_2 and hexagonal boron nitride (hBN) with adsorbed single adatoms (H, C, N, O, etc.), which can originate from molecules always present in the TEM column. We assess the ballistic displacement threshold energies T for the host atoms in 2D materials when adatoms are present and demonstrate that T can be reduced, as chemical bonds are locally weakened due to the formation of new bonds with the adatom. We further calculate the partial and total cross sections for atom displacement from MoS_2 and hBN, compare our results to the available experimental data, and conclude that adatoms should play a role in damage creation in MoS_2 and hBN sheets at electron energies below the knock-on threshold of the pristine system, thus mediating the buildup of electron beam-induced damage.

DOI: 10.1103/PhysRevMaterials.8.054004

I. INTRODUCTION

Transmission electron microscopy (TEM), including conventional TEM and scanning TEM (STEM), has proven to be one of the most powerful tools [1] to provide information on the atomic structure of materials with sub-Ångström resolution. Moreover, with the advent of aberration correctors and monochromators [2–6], the information on the local electronic [7], vibrational [8,9] and even magnetic [10] properties can be gained. The aberration-corrected TEM has allowed imaging of impurities [11–13] as well as intrinsic point defects [14–18] in bulk and two-dimensional (2D) materials and also made it possible to monitor their evolution in the real time.

However, it was realized long ago [19,20] that energetic electrons in the TEM interacting with the specimen can give rise to the formation of defects or even complete destruction of the sample. As the amount of damage is generally proportional to electron energy, limiting the undesirable effects of the beam has been one of the driving forces behind lowering the TEM operating voltage [6,21]. At the same time, defects can be created deliberately during the imaging, opening new routes in engineering the structure and properties of materials with atomic resolution [22,23]. All of these call upon complete understanding of how damage is created upon exposure to the electron beam in the TEM.

Three main mechanisms for material damage under an electron beam are the knock-on or ballistic damage, inelastic interactions, which involve electronic excitations and ionization, and beam-induced chemical etching, see Refs. [24–27] for an overview. Moreover, several mechanisms can simultaneously contribute to defect production [28,29].

The Coulomb interaction between the electrons and the atomic nuclei results in elastic scattering of the electrons. Putting aside light atoms, like hydrogen, electrons with relatively low kinetic energy (below 60 keV, but this is generally material dependent) do not result in enough recoil for the atoms in the specimen to be displaced. At higher energies the energy transfer can be high enough for atomic displacements. This mechanism of damage originating from kinetic energy transfer from high energy electrons to the target nuclei is the knock-on damage. The minimum electron energy required to cause displacement of atoms is referred to as electron "knock-on displacement threshold energy", which is related through the relativistic binary collision formula to the recoil atom displacement threshold energy T, that is the minimum kinetic energy the recoil atom should acquire to leave its position without immediate recombination. The knock-on displacement theory accounting also for lattice vibrations provided the dependence of the displacement cross-section on electron energy, which was in a very good agreement with the experimental data for the semimetallic graphene [30].

At the same time, for semiconducting/insulating 2D materials such as hexagonal boron nitride (hBN) [31], MoS_2 [28,32] and other transition metal dichalcogenides (TMDs) [33–35], metal phosphorous trisulfides (appearance of P vacancies) [36], the knock-on damage theory cannot describe the production of defects under low electron energy irradiation. This indicates that other damage mechanisms are active.

As shown recently [28], a combination of electronic excitations and knock-on damage can give rise to the displacement of atoms from 2D MoS_2 at electron energies well below the knock-on threshold. We note that electronic excitations/ionizations alone cannot result in the formation of defects in a perfect crystalline system with high electron mobility due to a quick delocalization of the excitation, as discussed previously [28] contrary to what happens in molecular crystals, where the electron excited into an antibonding state is normally localized on a specific bond. However, when a delocalized electronic excitation exists in a semiconducting material, it can localize on the emerging defect, such as a vacancy appearing at the position of the recoil atom, weakening the local chemical bonds and reducing the threshold energy [28,32]. Following this conjecture, Bui *et al.* [31] rationalized their experimental data obtained for hBN by fitting the displacement threshold values to the displacement cross sections scaled by the Bethe ionization cross section. The displacement thresholds were assessed by constraint density functional theory (DFT) molecular dynamics for (partially) ionized target atoms. This approach, which assumes localized ionization, is however not rigorous, as it contains parameters which are generally unknown. Moreover, the excitation/ionization efficiency should be smaller than the one required to provide an explanation for the damage production. Thus, other mechanisms likely contribute to the development of the sub-knock-on-threshold damage in hBN.

The third damage mechanism, beam-induced chemical etching, has received much less attention. It is active in graphene [37,38] and TMDs, see, e.g., Refs. [33,34]. The degradation of 2D $MoTe_2$ above oxygen partial pressure of 10^{-7} torr has been shown by in-situ TEM investigations [33]. Below this pressure, the material etching under the electron beam did not occur. Interestingly, the ubiquitous hydrocarbons accelerated the damage, by up to a factor of forty. In contrast to $MoTe_2$, MoS_2 was found to be inert under oxygen environment. These findings were rationalized through first-principles calculations by evaluating the potential barriers for the relevant chemical reactions. It was assumed that the radicals, that is adatoms, appear due to the splitting of the molecules by the electron beam, but the effects of the beam on the material with adatoms were not explicitly accounted for.

Here, using first-principles molecular dynamics we study how the presence of adatoms can affect ballistic damage creation in two representative 2D materials, MoS_2 and hBN. We calculate the ballistic displacement threshold energies T for the host atoms in 2D materials near adatoms and demonstrate that T can be reduced, as chemical bonds are locally weakened due to the formation of new bonds with the adatom. Using the McKinley-Feshbach formalism [39], we further calculate the cross sections for atom displacement from MoS_2 and hBN. The mechanism we discuss is different from the usual chemical etching which can be thermally activated and can proceed after the electron beam was switched off. It is based on ballistic energy transfer from the impinging electrons to the target atoms, but contrary to the conventional knock-on damage, in the presence of adatoms, which involves chemical effects and makes this channel dependent on adatom concentration.

II. COMPUTATIONAL DETAILS

All the calculations were performed within the framework of spin-polarized DFT and using plane-wave basis sets, as implemented in Vienna *Ab initio* Simulation Package [40,41]. The account for spin polarization is important to describe the energetics of the system with isolated atoms, as shown previously [42]. The semilocal functional of Perdew-Burke-Ernzerhof [43] was employed to describe exchange and correlations. The kinetic energy cutoff was set to 400 eV. The ionic and electronic convergence thresholds were set to 0.001 eV/Å and 10^{-5} eV, respectively.

Single layers of hBN and MoS_2 consisted of 100 and 90 atoms respectively. The adatom was placed on top of the sheet, and the geometry of the system was fully optimized. Then certain kinetic energy (energy close to the vacancy formation energy was normally chosen as a guess) was assigned to the recoil atom to mimic the nearly instantaneous momentum transfer from the impinging electron to the recoil atom [16,44–46], and evolution of the system in a microcanonical ensemble was simulated. The electronic system was assumed to be in the ground state, and the Born-Oppenheimer DFT molecular dynamics (BO DFT-MD) simulations were performed. Only the Γ-point was used to perform ground state DFT-MD.

Because the sheets of 2D materials are normally perpendicularly oriented to the beam direction, and for the energetic electrons the maximum energy/momentum transfer is in the forward direction, the initial velocity vector was chosen to be perpendicular to the 2D plane.

The displacement threshold energies T were defined as the minimum initial kinetic energy of the recoil atom required to sputter it. In practice the atom was deemed to be sputtered if its separation from the initial position was more than 4.5 Å. The initial kinetic energy was increased stepwise by 0.1 eV until the above criterion was met.

When the displacement threshold is known, the displacement cross section can be evaluated using the McKinley-Feshbach formalism [39] as a function of electron energy (and correspondingly, TEM voltage). Atomic vibrations lead to a smooth onset region of the displacement cross section, which extends to smaller electron energies as compared to the static case [24]. Out-of-plane vibrations were estimated within the Debye model employing Debye temperature 262.3 K [47] and 400 K [48] for MoS_2 and hBN, respectively. We note the cross section can be directly measured in the TEM experiments by counting the number of missing atoms [16,28,31,32].

The following equation was used for calculating the total displacement cross section σ_{tot} of the atoms as a function of electron energy E:

$$\sigma_{tot}(E) = \sigma(E)(1-\chi) + \sigma_{ad}(E)\chi, \tag{1}$$

where σ is the displacement cross section calculated for the pristine system (without adsorbed adatoms) and σ_{ad} is the displacement cross section for the system with adsorbed adatoms. χ is the ratio of the number of adatoms to the number of surface atoms in the material (relative atomic concentration of adatoms).

TABLE I. S vacancy formation and displacement threshold energies for MoS_2 in the H phase with and without adsorbed adatoms on the surface. E_f^V is the vacancy formation energy. $T_A[X]$ is the displacement threshold energy for a material atom (X = S) with an adatom A nearby, and $T[A]$ is the energy needed to remove the adatom A from MoS_2. All energies are in eV.

Adatom (A)	E_f^V	$T_A[X]$	$T[A]$
None	6.07	6.6	
H	2.98	3.4	1.1
C	0.59	2.7	2.5
O	2.82	> 6.6	
N	2.17	> 6.6	
S	3.34	> 6.6	
Si	1.34	> 6.6	

Vacancy formation energy (E_f^V) was assessed as

$$E_f^V = (E_{N-1} + E_{\text{iso}}) - E_N, \tag{2}$$

where E_{N-1} and E_N are the total energies of the defective and the pristine system (composed from N atoms), respectively, and E_{iso} is the energy of an isolated atom. We note that this equation cannot be used to assess the formation energy and equilibrium concentration of defects, but gives the energy required to move an atom to infinity, which physically corresponds to the sputtering process.

Adatom adsorption energy was evaluated through

$$E_{ad} = E_{N+1} - (E_{\text{iso}} + E_N), \tag{3}$$

where E_{N+1} is the total energy of the system with the adsorbed adatom.

III. RESULTS AND DISCUSSIONS

A. Displacement of S atoms from MoS_2 by the electron beam when adatoms are present

As the displacement threshold energies are related to the vacancy formation energies E_f^V [49], we first assessed how the formation energies of S vacancies change when the S atom is removed together with the adatom (such as H, C, O, N, S, Si) as a dimer, as schematically illustrated in Fig. 1. The results are presented in Table I. Here we use the following notations: $T_A[X]$ denotes the displacement threshold energy of target atom [X] (here X=S) with nearby adatoms (A = C, H). The term in brackets indicates the atom to which energy is transferred from the impinging electron. Therefore, $T[A]$ denotes the energy necessary to sputter the adatom from the surface of the host material.

It is evident that E_f^V is reduced for all considered adatoms as compared to the pristine system (without adatoms). This is an expected result, as the chemical potential of the free-standing S atom is obviously higher than in the dimer, and at the same time the chemical bonding between the S atom in MoS_2 and the adatom should be weaker than in the dimer, where more electrons are available for bonding. This may result in lower displacement thresholds, especially if the adatoms are light atoms.

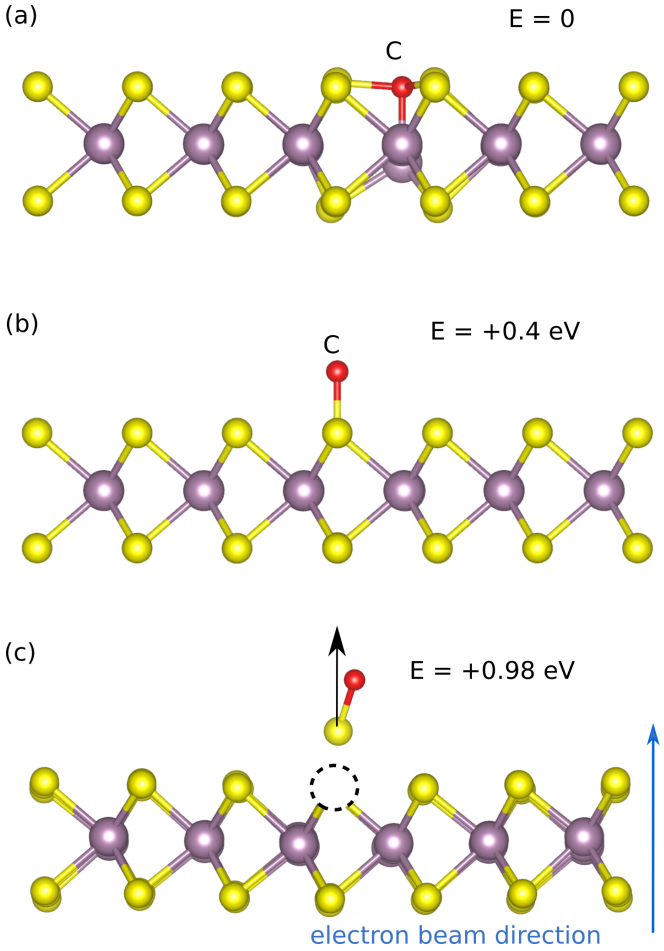

FIG. 1. Atomic structures of MoS_2 sheet with carbon adatom adsorbed (a) on top of Mo atom and (b) on top of S atom. (c) The recoil S atom in the presence of C adatom is displaced together with the adatom forming a dimer. For each case, the relative energy difference with respect to the lowest energy configuration is given.

The displacement threshold energies T were then computed using DFT MD for the host atoms neighboring the adatoms. The results are also presented in Table I. For the pristine system $T[S] = 6.6$ eV. We note that the recoil atom can be sputtered together with the adatom forming a dimer, or as a single atom. For all adatoms, except for H and C, the values of T proved to be higher than that for the pristine system, as the initial energy/momentum was transferred from the energetic electron to the recoil S atom and the adatom. Because we are primarily interested in the formation of defects below the knock-on threshold of atoms in the pristine system, in what follows, we discuss H and C adatoms only, no defect production for other adatoms is expected at electron energies close to the displacement threshold of S atoms from the pristine system.

1. C adatoms on MoS_2

Our calculations indicated that C adatoms can exist on MoS_2 in two stable configurations, on top of a Mo and S atom, Fig. 1, with the latter configuration being higher in energy by about 0.4 eV. Using nudged elastic band theory, the

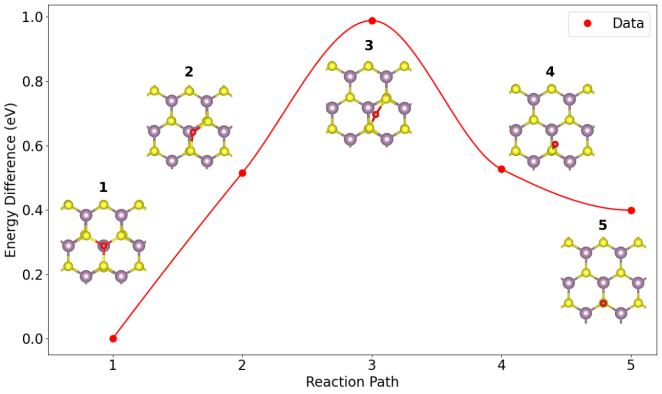

FIG. 2. Energy profile for a diffusion of the adsorbed C from top of Mo atom position (1) to top of S atom position (5) using nudged elastic band theory.

energy barrier of about 1 eV for C diffusion on MoS_2 from the position on top of Mo site (1) to the position on top of S site (5) was calculated. The diffusion pathway is shown in Fig. 2. It is evident from the plot that the position on top of S atom is metastable with a barrier of about 0.6 eV. These results indicate that, on the one hand, the C atom can easily be pushed into the metastable configuration due to electron impacts, and on the other hand, can exist in this configuration for a macroscopically long time at room temperature (of about 0.01 second) and be sputtered away or return into the lowest energy configuration by another energetic electron.

T_C[S] were calculated for both configurations. The recoil S atom was found to move together with the C atom as a dimer, Fig. 1(c). T_C[S] proved to be much lower for the metastable configuration shown in Fig. 1(b) than for the lowest energy configuration, Fig. 1(a), and also lower than that for the pristine system. Specifically, $T_C[S] = 2.7$ eV is much less than the value of $T[S] = 6.6$ eV for the pristine case, when no adatom is present. We note that although the barrier for diffusion of adatoms can be lower than the displacement thresholds of the nearby host atoms and their diffusivity can increase under electron beam, the adatoms would still move randomly and as momentum transfer occurs much faster than any atomic jumps, the defect formation process will not be affected by the adatom jumps, only the location of defects will be different.

As adatoms can also be displaced by direct electron impacts, we also calculated the displacement threshold T[C] for the C adatom. We found that $T[C] = 2.5$ eV is rather low, which can give rise to a large displacement cross section as discussed later on.

2. *H adatoms on* MoS_2

The lowest energy position of H adatoms is on top of the S atoms. Similar to C adatoms, the recoil S atom is displaced together with the H adatom, so that the dimer is sputtered away. Our calculations gave a value of $T_H[S] = 3.4$ eV. The displacement threshold energy for the adatom alone ($T[H] = 1.1$ eV) was found to be much less than T_H[S] value, indicating that H adatoms can easily be sputtered away.

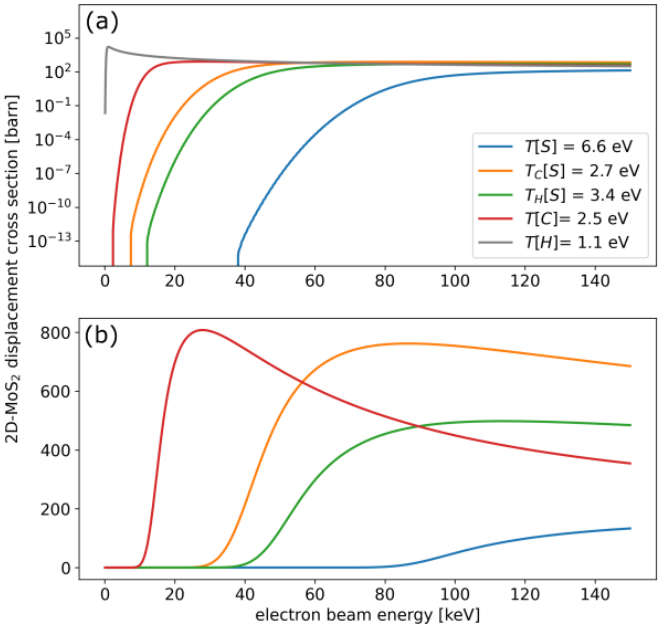

FIG. 3. Displacement cross sections of S atoms and C, H adatoms from MoS_2 in the logarithmic (a) and linear (b) scales. The calculated displacement threshold energies T_A[X] and energies needed to sputter the adatoms T[A] are also listed in (a). The term in brackets denotes the atom to which energy is transferred from the impinging electron, X is the target atom and A stands for the adatom in its vicinity. The cross section for H adatom is not shown in (b).

3. *Cross sections for adatoms and host S atom sputtering in the presence of adatoms within the framework of the McKinley-Feshbach formalism*

Having computed the threshold displacement energies, we calculated the individual cross sections for each process. In Fig. 3(a), cross sections for displacing S atoms in the presence of adatoms and adatoms themselves are shown using the

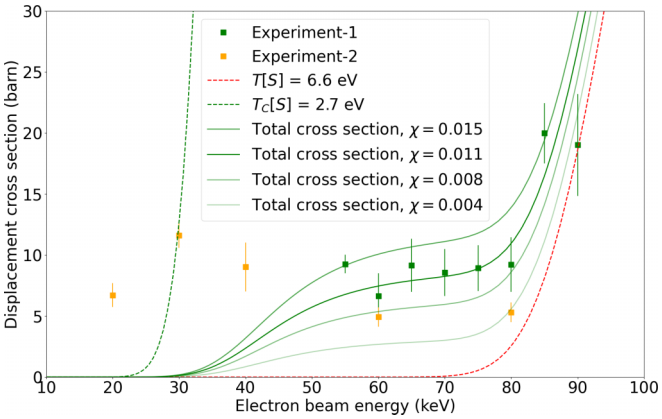

FIG. 4. Experimental and theoretical displacement cross sections for S atoms from MoS_2. The data points stand for experimentally determined cross section (Experiment-1 [32], Experiment-2 [28]). The dashed green and red lines correspond to the displacement cross sections σ_{ad} and σ with and without adatoms, respectively. The solid green lines correspond to theoretical total cross section σ_{tot} at different adatom concentrations χ.

TABLE II. Vacancy formation and displacement threshold energies for boron (B) atoms in hBN with and without adatoms on the surface. $T_A[X']$ is the displacement threshold energy when electron beam direction is reversed, so that the adatom and the electron beam source are on the same side of the hBN sheet. $T_X[A']$ is the displacement threshold energy for a head-on collision between the adatom with the underlying material atom. In the latter process, it is assumed that the electron collides with the adatom on the side of hBN facing the electron beam.

Adatom (A)	E_f^V	$T_A[X]$	$T_A[X']$	$T_X[A']$	$T[A]$
None	16.4	19			
H	12.96	17		68	0.5
C	12.7	16	16		2.0
N	11.8	18			
O	9.34	18			
F	10.43	> 19			

logarithmic scale. For the sake of comparison, the results for the pristine system are also presented.

It is evident that the presence of adatoms can dramatically increase the probability of displacement of the S atom neighboring the adatom (the yellow curves in Fig. 3), and that it can happen at much lower energies than in the pristine material. At the same time, the cross section for sputtering H atoms is rather high, so that such adatoms, even if originally present on the side of MoS_2 sheet opposite to the beam source, will be very quickly removed by the electron beam at electron energies below 70 keV. Thus one can conclude that H adatoms will not substantially contribute to the formation of S vacancies in MoS_2 under the electron beam in this energy range.

For the C adatom, however, the situation is different. The cross sections for removing the C adatom and S atom next to C atoms are comparable, Fig. 3(b), so that C adatoms can give rise to the formation of vacancies. The calculated displacement threshold energies for S atom in the pristine system is around 70 keV, for S atom with an adsorbed C adatom is around 20 keV. It is important to emphasize that the presented cross sections are meaningful only if the relative concentration χ of atoms (adatoms) is accounted for, and to quantify the damage, the cross section must be weighted using Eq. (1).

In Fig. 4, we compare the experimental (taken from Refs. [32] and [28]) and total displacement cross section calculated through Eq. (1) using different values of χ. Putting aside the low energy (below 50 keV) limit, where electronic excitations can contribute [28], most of the experimental data points fit within error bars for a χ value of 0.011. This is a reasonable value, as a substantial part of MoS_2 sheets can be covered with amorphous carbon or hydrocarbons after transfer to the TEM grid. We stress, however, that our goal is not to find the best fit to the experimental results, but discuss the mechanisms which can contribute to the damage formation under the electron beam, especially at electron voltages below the ballistic displacement threshold.

TABLE III. Vacancy formation and displacement threshold energies for nitrogen (N) atoms in hBN with and without adatoms on the surface.

Adatom (A)	E_f^V	$T_A[X]$	$T_A[X']$	$T_X[A']$	$T[A]$
None	12.9	19.4			
H	9.06	19		89	0.1
C	5.67	> 19.4	15		2.0
O	7.49	> 19.4			
S	8.12	> 19.4			
Cl	9.98	> 19.4			

B. Displacement of atoms from hBN sheets by the electron beam when adatoms are present

Similar to MoS_2, we added single atoms to hBN and calculated vacancy formation energies when these atoms are adsorbed on hBN. The results are presented in Table II and III. The vacancy formation energy decreases in all cases when adatoms are present on the surface. Then using DFT MD we calculated displacement threshold values $T_A[X]$ (A = H, C, N, O, S, F, Cl, X = B, N). We found that $T_A[X]$ does not noticeably decrease, except for H and C adatoms, where displacement thresholds decrease by up to 3 eV. Thus in what follows, we concentrate on H and C adatoms.

1. H adatoms on h-BN

The optimized atomic structure for H atoms adsorbed on top of B atom is shown in Fig. 5(a). The adsorption energy was found to be -0.04 eV, which is very small, indicating a weak bonding. Even weaker interaction was found for H atoms on top of N atoms. The low adsorption energies are in agreement with the results of previous calculations, see Refs. [50,51] and references therein. Low adsorption energies indicate that the adatoms can be highly mobile, as thermally activated diffusion and desorption/adsorption are very likely. However, this would not affect the mechanism described here: Even mobile adatoms will spend most of the time bound to one adsorption site, with occasional thermally activated jumps to a neighboring site. Hence, on the time scale of the electron impact and the following dynamics, they can be considered as stationary.

In Tables II and III, we list displacement threshold energies $T_H[X]$ and $T_H[X']$ for H on hBN. The $T_H[B]$ and $T_H[N]$ are the displacement threshold energies of B/N atoms when adatoms are adsorbed on the opposite side of the material with respect to incoming electron beam direction, Fig. 5(b). Similarly, $T_H[B']$ and $T_H[N']$ are the threshold values for B/N atoms when adatoms are adsorbed on the side of the material facing the electron source, Fig. 5(c).

$T_H[B]$ and $T_H[N]$ are 17 and 19 eV, respectively. Hence, the threshold values decrease only slightly in this particular scenario when H is adsorbed on top of hBN. Moreover, the $T[H]$ is in the range of 0.1–0.5 eV, which indicates that H adatoms on the side opposite to the electron beam will immediately be displaced by the impinging electrons.

However, one more process is possible: a ballistic collision of the electron with the H adatom on the side of hBN facing the beam, followed by a head-on collision of the H atom with the host atom. Our DFT MD simulations gave values of $T_B[H'] = 68$ eV and $T_N[H'] = 89$ eV, respectively, which, as discussed below, corresponds to rather low electron beam

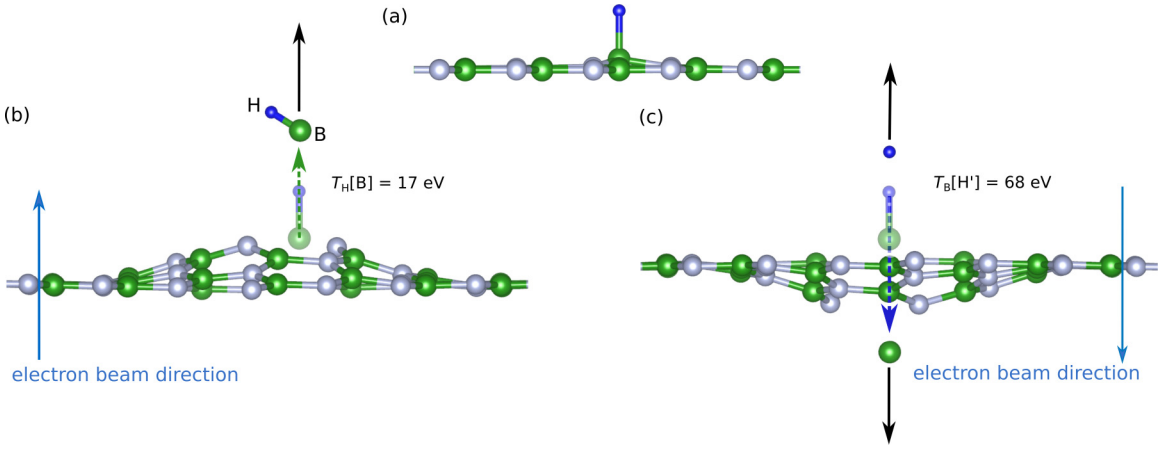

FIG. 5. Mechanisms of target atom displacement when H adatoms are present on hBN. (a) Start configuration: atomic structure of H adatom adsorbed on top of boron atom. (b) H adatom on side opposite to electron beam direction: displacement of boron atom with H adatom attached. (c) H adatom facing the electron beam: H atom receives energy from the electron and undergoes head-on collision with the boron atom.

energies $E \sim M_p T_X[H']/4m_e \sim 30$ keV, as follows from the classical binary collision formula. Here, M_p is the mass of H atom and m_e is the electron mass.

2. C adatoms on h-BN

In case of C adatoms on hBN, we have considered two possibilities as shown in Fig. 6(a) and 6(b). In both cases, B/N atoms can be displaced by the electron beam. The first possibility is when an adatom is adsorbed on the opposite side of the material with regard to the beam source. The threshold corresponding to this case is written as T_C[B] and T_C[N] for B/N atom. In the second case, the beam source and the adatom are positioned on the same side. In this case, notations $T_C[B']$ and $T_C[N']$ are used. The values for T_C[B] and $T_C[B']$ are both equal to 16 eV, which is 3 eV less than those in the pristine hBN. On the contrary, T_C[N] is higher than for that for the pristine system. $T_C[N'] = 15$ eV, which is 4.4 eV less than in the pristine hBN case.

C adatoms can also be displaced by the beam, and the calculations of the displacement threshold gave T[C] = 2.0 eV (the adatom is on the other side of the sheet than the electron source, Fig. 6, which can give rise to a large displacement cross section and quick sputtering of the adatoms on the side of h-BN opposite to the beam source). However, the C adatom can stay on the hBN surface facing the beam source.

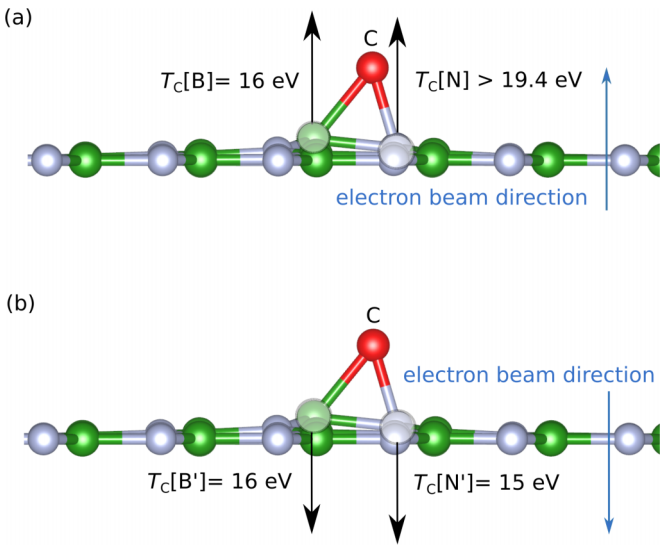

FIG. 6. Atomic structure of C adatoms adsorbed on hBN. (a) The arrows indicate the initial velocities of the recoil B/N atoms when the C adatom is on the opposite side of the sheet with respect to incoming electron beam direction. (b) C adatom positioned on the same side of hBN as the beam source.

3. Cross sections for B/N atoms sputtering in the presence of adatoms within the framework of the McKinley-Feshbach formalism

We first analyzed the effects of C adatoms on the displacement cross sections. Figure 7(a) shows the calculated cross sections for B atoms when C and H atoms are adsorbed on hBN. It is evident that the threshold is around 65 keV when C adatom is adsorbed while without C adatoms, it is around 77 keV. By varying χ values, that is the concentration of adatoms, a set of curves can be produced, Fig. 7(b), but none of the results for C adatoms would match the experimental cross section data taken from Ref. [31].

Figure 8(a) shows the cross sections when N atoms are displaced from hBN in the presence of C adatoms. The threshold is around 76 keV, noticeably smaller as compared to the theoretical value for the pristine material (100 keV). From the comparison of the theoretical total displacement cross sections with the experimental data shown in Fig. 8(b), it is evident that there is an agreement for value of χ around 0.2. Again, not all the data points are matched perfectly. However, we do see a trend of reduction of threshold values in both B/N atom when C is adsorbed on hBN. From the comparison of the theoretical total displacement cross section with the experimental data, one can conclude that the quick increase in the cross section at $\chi \sim 0.2$ can be explained by the presence of C

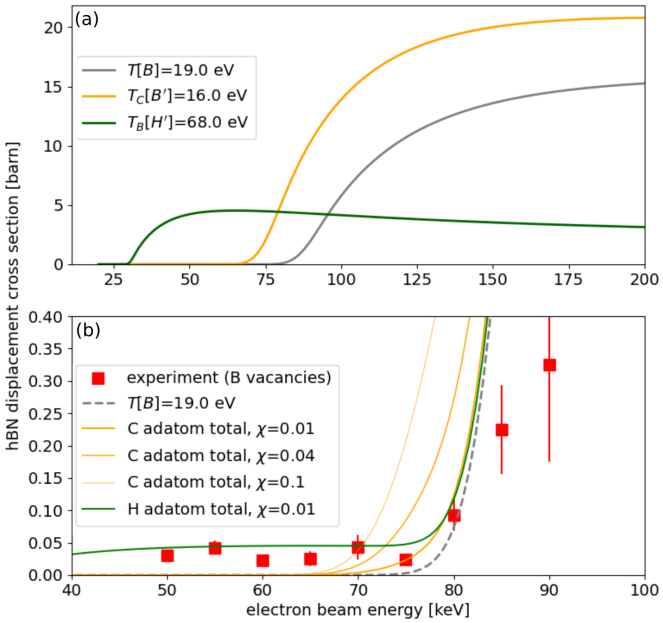

FIG. 7. Displacement cross sections for B atoms in hBN as functions of electron beam energy (a) and those for energies below 100 keV (b). The displacement cross sections for B atoms in a pristine material, in the presence C and H adatoms are shown in grey, yellow, and green, respectively. The experimental data points [31] are added to (b) along with the total cross sections at different concentrations of C and H adatoms.

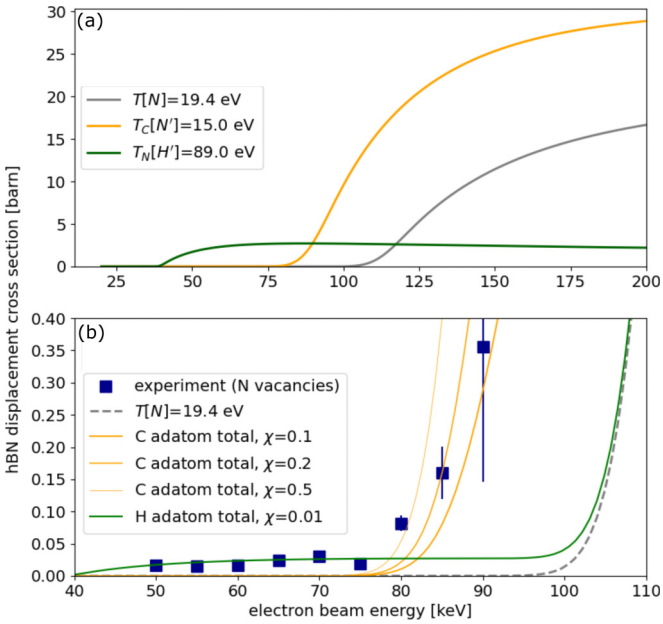

FIG. 8. Displacement cross sections for N atoms in hBN as functions of electron beam energy (a) and those for energies below 100 keV (b). The displacement cross sections for B atoms in a pristine material, in the presence C and H adatoms are shown in grey, yellow, and green, respectively. The experimental data points [31] are added to (b) along with the total cross sections at different concentrations of C and H adatoms.

adatoms, but not the low-energy tail. Moreover, it is important to mention that sputtering of B/N atoms in the presence of C adatoms does not necessarily result in the formation of vacancies, as C atoms can take the position of sputtered atoms at the B/N vacancy site [52,53]. Since the experimental cross section is based on the B/N monovacancy counts in hBN, the direct comparison of the calculated cross section with the experiment is not possible. The information on substitution of C at B/N vacancy site and loss of B/N atoms from hBN can also be determined from electron-energy-loss spectroscopy and slight contrast changes [54,55].

At the same time, the account for the double collision process involving H adatoms on the side of the hBN sheet facing the beam source and values of $T_B[H']$, Fig. 7(a), and $T_N[H']$, Fig. 8(a), indicates that displacement of host atoms from hBN is possible at electron energies around 30/40 keV. The effective concentration of H adatoms should be around 1% in order to explain the experimental data, but this is just an order of magnitude estimate, as at finite temperatures adatoms can move and be not exactly on top of the host B/N atoms, so that energy transfer could be different.

IV. CONCLUSIONS

In conclusion, by employing DFT MD and taking MoS_2 and hBN as typical 2D materials, we studied how adatoms, which are always present on the surface of 2D materials in the TEM, can contribute to the development of the beam-induced damage in the target. We assessed first the ballistic displacement threshold energies for the host atoms neighboring the adatoms and demonstrated that they can be reduced if H and C adatoms are present, as chemical bonds in the materials are locally weakened due to the formation of new bonds with the adatom. Then using the McKinley-Feshbach formalism we computed the partial and total cross sections for atom displacement from MoS_2 and hBN and compared our results to the available experimental data. Our results indicate that the presence of adatoms can give rise to damage creation in MoS_2 and hBN sheets at electron energies below the knock-on threshold for the pristine material. This process is different from the usual chemical etching which can be thermally activated and can proceed after the electron beam was switched off. The process originates from the ballistic energy transfer from the impinging electrons to the target atoms, but contrary to the conventional knock-on damage, requires the presence of adatoms, which makes this channel dependent on adatom concentration and strength of chemical bonding. We note that adatoms can also be created by the electron beam due to the splitting of ubiquitous water and hydrocarbon molecules. Moreover, the probability for splitting the molecules decreases with electron beam energy (for energies above 10 keV), which may give rise to concentration of adatoms dependent on beam energy, in addition to vacuum level. We stress, however, that concentration of H/C atoms can hardly be defined in the experiment, as they normally migrate rather fast over the surface of 2D materials, especially under electron beam. We also note that the presence of adatoms will likely give rise to the formation of in-gap defect states, which in turn might affect the localization of

beam-induced excitations and further lower the displacement threshold, as discussed previously [28].

Our results can provide complementary data or even an alternative explanation for the experimental results reported by Bui *et al.* [31] for damage production in hBN in the presence of C and H adatoms rather than ionization of the target atoms and also hint at an additional channel of defect production in MoS_2 under electron beam at energies below the knock-on threshold [28,32]. A quantitative agreement with the experimental data can be achieved for reasonable adatom concentration, but unfortunately both models (electronic excitations and adatom-mediated knock-on damage) have uncontrollable parameters. Anyway, the main goal of this work is not to find the best fit to the experimental results, but outline the mechanisms which can contribute to damage formation at electron energies below the knock-on displacement threshold when adatoms are present.

ACKNOWLEDGMENTS

We acknowledge funding from the German Research Foundation (DFG), Projects No. KR 4866/9-1 and No. ME 3133/6-1, and the collaborative research center "Chemistry of Synthetic 2D Materials" CRC-1415-417590517. Generous CPU time grants from the Technical University of Dresden computing cluster (TAURUS) and Gauss Centre for Supercomputing e.V [56]. Supercomputer HAWK at Höchstleistungsrechenzentrum Stuttgart [57] are greatly appreciated. We further thank T. Susi, J. Kotakoski, and K. Suenaga for fruitful discussions.

[1] S. J. Pennycook, The impact of STEM aberration correction on materials science, Ultramicroscopy **180**, 22 (2017).

[2] H. Rose, Outline of a spherically corrected semi-aplanatic medium-voltage tem, Optik **85**, 19 (1990).

[3] M. Haider, S. Uhlemann, E. Schwan, H. Rose, B. Kabius, and K. Urban, Electron microscopy image enhanced, Nature (London) **392**, 768 (1998).

[4] O. L. Krivanek, N. Dellby, and A. R. Lupini, Towards sub-Å electron beams, Ultramicroscopy **78**, 1 (1999).

[5] R. Erni, M. D. Rossell, C. Kisielowski, and U. Dahmen, Atomic-resolution imaging with a sub-50-pm electron probe, Phys. Rev. Lett. **102**, 096101 (2009).

[6] M. Linck, P. Hartel, S. Uhlemann, F. Kahl, H. Müller, J. Zach, M. Haider, M. Niestadt, M. Bischoff, J. Biskupek, Z. Lee, T. Lehnert, F. Börrnert, H. Rose, and U. Kaiser, Chromatic aberration correction for atomic resolution TEM imaging from 20 to 80 kv, Phys. Rev. Lett. **117**, 076101 (2016).

[7] P. K. Gogoi, Y.-C. Lin, R. Senga, H.-P. Komsa, S. L. Wong, D. Chi, A. V. Krasheninnikov, L.-J. Li, M. B. H. Breese, S. J. Pennycook, A. T. S. Wee, and K. Suenaga, Layer rotation-angle-dependent excitonic absorption in van der Waals heterostructures revealed by electron energy loss spectroscopy, ACS Nano **13**, 9541 (2019).

[8] O. Krivanek, T. C. Lovejoy, N. Dellby, T. Aoki, R. W. Carpenter, P. Rez, E. Soignard, J. Zhu, P. E. Batson, M. J. Lagos, R. F. Egerton, and P. a. Crozier, Vibrational spectroscopy in the electron microscope, Nature (London) **514**, 209 (2014).

[9] R. Senga, K. Suenaga, P. Barone, S. Morishita, F. Mauri, and T. Pichler, Position and momentum mapping of vibrations in graphene nanostructures, Nature (London) **573**, 247 (2019).

[10] Y.-C. Lin, P.-Y. Teng, P.-W. Chiu, and K. Suenaga, Exploring the single atom spin state by electron spectroscopy, Phys. Rev. Lett. **115**, 206803 (2015).

[11] U. Bangert, A. Stewart, E. O'Connell, E. Courtney, Q. Ramasse, D. Kepaptsoglou, H. Hofsäss, J. Amani, J. S. Tu, and B. Kardynal, Ion-beam modification of 2-D materials - single implant atom analysis via annular dark-field electron microscopy, Ultramicroscopy **176**, 31 (2017).

[12] A. W. Robertson, Y. C. Lin, S. Wang, H. Sawada, C. S. Allen, Q. Chen, S. Lee, G. D. Lee, J. Lee, S. Han, E. Yoon, A. I. Kirkland, H. Kim, K. Suenaga, and J. H. Warner, Atomic structure and spectroscopy of single metal (Cr, V) substitutional dopants in monolayer MoS_2, ACS Nano **10**, 10227 (2016).

[13] R. Luo, M. Gao, C. Wang, J. Zhu, R. Guzman, and W. Zhou, Probing functional structures, defects, and interfaces of 2D transition metal dichalcogenides by electron microscopy, Adv. Funct. Mater. **34**, 2307625 (2024).

[14] W. Zhou, X. Zou, S. Najmaei, Z. Liu, Y. Shi, J. Kong, J. Lou, P. M. Ajayan, B. I. Yakobson, and J.-C. Idrobo, Intrinsic structural defects in monolayer molybdenum disulfide, Nano Lett. **13**, 2615 (2013).

[15] O. S. Ovchinnikov, A. O'Hara, S. Jesse, B. M. Hudak, S. Yang, A. R. Lupini, M. F. Chisholm, W. Zhou, S. V. Kalinin, A. Y. Borisevich, and S. T. Pantelides, Detection of defects in atomic-resolution images of materials using cycle analysis, Adv. Struct. Chem. Imaging **6**, 3 (2020).

[16] H.-P. Komsa, J. Kotakoski, S. Kurasch, O. Lehtinen, U. Kaiser, and A. V. Krasheninnikov, Two-dimensional transition metal dichalcogenides under electron irradiation: Defect production and doping, Phys. Rev. Lett. **109**, 035503 (2012).

[17] J. C. Meyer, A. Chuvilin, G. Algara-Siller, J. Biskupek, and U. Kaiser, Selective sputtering and atomic resolution imaging of atomically thin boron nitride membranes, Nano Lett. **9**, 2683 (2009).

[18] G.-D. Lee, C. Z. Wang, E. Yoon, N.-M. Hwang, D.-Y. Kim, and K. M. Ho, Diffusion, coalescence, and reconstruction of vacancy defects in graphene layers, Phys. Rev. Lett. **95**, 205501 (2005).

[19] O. Scherzer, Die Strahlenschädigung der Objekte als Grenze für die hochauflösende Elektronenmikroskopie, Berichte der Bunsengesellschaft für physikalische Chemie **74**, 1154 (1970).

[20] F. Banhart, Irradiation effects in carbon nanostructures, Rep. Prog. Phys. **62**, 1181 (1999).

[21] R. F. Egerton, Choice of operating voltage for a transmission electron microscope, Ultramicroscopy **145**, 85 (2014).

[22] A. V. Krasheninnikov and F. Banhart, Engineering of nanostructured carbon materials with electron or ion beams, Nat. Mater. **6**, 723 (2007).

[23] X. Zhao, J. Kotakoski, J. C. Meyer, E. Sutter, P. Sutter, A. V. Krasheninnikov, U. Kaiser, and W. Zhou, Engineering and modifying two-dimensional materials by electron beams, MRS Bull. **42**, 667 (2017).

[24] T. Susi, J. C. Meyer, and J. Kotakoski, Quantifying transmission electron microscopy irradiation effects using two-dimensional materials, Nat. Rev. Phys. **1**, 397 (2019).

[25] R. F. Egerton, P. Li, and M. Malac, Radiation damage in the TEM and SEM, Micron **35**, 399 (2004).

[26] R. F. Egerton, Control of radiation damage in the TEM, Ultramicroscopy **127**, 100 (2013).

[27] N. Jiang, Electron beam damage in oxides: A review, Rep. Prog. Phys. **79**, 016501 (2016).

[28] S. Kretschmer, T. Lehnert, U. Kaiser, and A. V. Krasheninnikov, Formation of defects in two-dimensional MoS_2 in the transmission electron microscope at electron energies below the knock-on threshold: The role of electronic excitations, Nano Lett. **20**, 2865 (2020).

[29] T. Lehnert, O. Lehtinen, G. Algara-Siller, and U. Kaiser, Electron radiation damage mechanisms in 2D $MoSe_2$, Appl. Phys. Lett. **110**, 033106 (2017).

[30] J. C. Meyer, F. Eder, S. Kurasch, V. Skakalova, J. Kotakoski, H. J. Park, S. Roth, A. Chuvilin, S. Eyhusen, G. Benner, A. V. Krasheninnikov, and U. Kaiser, Accurate measurement of electron beam induced displacement cross sections for single-layer graphene, Phys. Rev. Lett. **108**, 196102 (2012).

[31] T. A. Bui, G. T. Leuthner, J. Madsen, M. R. A. Monazam, A. I. Chirita, A. Postl, C. Mangler, J. Kotakoski, and T. Susi, Creation of single vacancies in hBN with electron irradiation, Small **19**, 2301926 (2023).

[32] C. Speckmann, J. Lang, J. Madsen, M. R. A. Monazam, G. Zagler, G. T. Leuthner, N. McEvoy, C. Mangler, T. Susi, and J. Kotakoski, Combined electronic excitation and knock-on damage in monolayer MoS_2, Phys. Rev. B **107**, 094112 (2023).

[33] E. H. Åhlgren, A. Markevich, S. Scharinger, B. Fickl, G. Zagler, F. Herterich, N. McEvoy, C. Mangler, and J. Kotakoski, Atomic-scale oxygen-mediated etching of 2D MoS_2 and $MoTe_2$, Adv. Mater. Interfaces **9**, 2200987 (2022).

[34] A. K. Dash, H. Swaminathan, E. Berger, M. Mondal, T. Lehenkari, P. R. Prasad, K. Watanabe, T. Taniguchi, H.-P. Komsa, and A. Singh, Evidence of defect formation in monolayer MoS_2 at ultralow accelerating voltage electron irradiation, 2D Mater. **10**, 035002 (2023).

[35] Y. C. Lin, T. Björkman, H. P. Komsa, P. Y. Teng, C. H. Yeh, F. S. Huang, K. H. Lin, J. Jadczak, Y. S. Huang, P. W. Chiu, A. V. Krasheninnikov, and K. Suenaga, Three-fold rotational defects in two-dimensional transition metal dichalcogenides, Nat. Commun. **6**, 6736 (2015).

[36] J. Köster, A. Storm, M. Ghorbani-Asl, S. Kretschmer, T. E. Gorelik, A. V. Krasheninnikov, and U. Kaiser, Structural and chemical modifications of few-layer transition metal phosphorous trisulfides by electron irradiation, J. Phys. Chem. C **126**, 15446 (2022).

[37] G. T. Leuthner, S. Hummel, C. Mangler, T. J. Pennycook, T. Susi, J. C. Meyer, and J. Kotakoski, Scanning transmission electron microscopy under controlled low-pressure atmospheres, Ultramicroscopy **203**, 76 (2019).

[38] B. Sommer, J. Sonntag, A. Ganczarczyk, D. Braam, G. Prinz, A. Lorke, and M. Geller, Electron-beam induced nano-etching of suspended graphene, Sci. Rep. **5**, 7781 (2015).

[39] W. A. McKinley and H. Feshbach, The Coulomb scattering of relativistic electrons by nuclei, Phys. Rev. **74**, 1759 (1948).

[40] G. Kresse and J. Hafner, *Ab initio* molecular dynamics for liquid metals, Phys. Rev. B **47**, 558 (1993).

[41] G. Kresse and J. Furthmüller, Efficiency of *ab initio* total energy calculations for metals and semiconductors using a plane-wave basis set, Comput. Mater. Sci. **6**, 15 (1996).

[42] S. Kretschmer, S. Ghaderzadeh, S. Facsko, and A. V. Krasheninnikov, Threshold ion energies for creating defects in 2D materials from first-principles calculations: Chemical interactions are important, J. Phys. Chem. Lett. **13**, 514 (2022).

[43] J. P. Perdew, K. Burke, and M. Ernzerhof, Generalized gradient approximation made simple [Phys. Rev. Lett. **77**, 3865 (1996)], Generalized gradient approximation made simple Phys. Rev. Lett. **78**, 1396(E) (1997).

[44] A. Yoshimura, M. Lamparski, N. Kharche, and V. Meunier, First-principles simulation of local response in transition metal dichalcogenides under electron irradiation, Nanoscale **10**, 2388 (2018).

[45] M. Pizzochero and O. V. Yazyev, Single-layer 1T'-MoS_2 under electron irradiation from *ab initio* molecular dynamics, 2D Mater. **5**, 025022 (2018).

[46] O. Cretu, H.-p. Komsa, O. Lehtinen, G. Algara-Siller, U. Kaiser, K. Suenaga, and A. V. Krasheninnikov, Experimental observation of boron nitride chains, ACS Nano **8**, 11950 (2014).

[47] B. Peng, H. Zhang, H. Shao, Y. Xu, X. Zhang, and H. Zhu, Thermal conductivity of monolayer MoS_2, $MoSe_2$, and WS_2: Interplay of mass effect, interatomic bonding and anharmonicity, RSC Adv. **6**, 5767 (2016).

[48] T. Tohei, A. Kuwabara, F. Oba, and I. Tanaka, Debye temperature and stiffness of carbon and boron nitride polymorphs from first-principles calculations, Phys. Rev. B **73**, 064304 (2006).

[49] F. Banhart, J. X. Li, and A. V. Krasheninnikov, Carbon nanotubes under electron irradiation: Stability of the tubes and their action as pipes for atom transport, Phys. Rev. B **71**, 241408(R) (2005).

[50] Z. Zhou, J. Zhao, Z. Chen, X. Gao, T. Yan, B. Wen, and P. v. R. Schleyer, Comparative study of hydrogen adsorption on carbon and Bn nanotubes, J. Phys. Chem. B **110**, 13363 (2006).

[51] K. R. Koswattage, I. Shimoyama, Y. Baba, T. Sekiguchi, and K. Nakagawa, Selective adsorption of atomic hydrogen on a *h* -BN thin film, J. Chem. Phys. **135**, 014706 (2011).

[52] O. L. Krivanek, M. F. Chisholm, V. Nicolosi, T. J. Pennycook, G. J. Corbin, N. Dellby, M. F. Murfitt, C. S. Own, Z. S. Szilagyi, M. P. Oxley, S. T. Pantelides, and S. J. Pennycook, Atom-by-atom structural and chemical analysis by annular dark-field electron microscopy, Nature (London) **464**, 571 (2010).

[53] N. Berseneva, A. V. Krasheninnikov, and R. M. Nieminen, Mechanisms of postsynthesis doping of boron nitride nanostructures with carbon from first-principles simulations, Phys. Rev. Lett. **107**, 035501 (2011).

[54] J. C. Meyer, S. Kurasch, H. J. Park, V. Skakalova, D. Künzel, A. Gross, A. Chuvilin, G. Algara-Siller, S. Roth, T. Iwasaki, U. Starke, J. H. Smet, and U. Kaiser, Experimental analysis of charge redistribution due to chemical bonding by high-resolution transmission electron microscopy, Nat. Mater. **10**, 209 (2011).

[55] X. Wei, M.-S. Wang, Y. Bando, and D. Golberg, Electron-beam-induced substitutional carbon doping of boron nitride nanosheets, nanoribbons, and nanotubes, ACS Nano **5**, 2916 (2011).

[56] www.gauss-centre.eu.

[57] www.hlrs.de.